Journal of Nuclear Materials 389 (2009) 288–296

Contents lists available at ScienceDirect

Journal of Nuclear Materials

journal homepage: www.elsevier.com/locate/jnucmat

Materials researches at the Paul Scherrer Institute for developing high power spallation targets

Yong Dai *, Werner Wagner

Spallation Neutron Source Division, Paul Scherrer Institut, 5232 Villigen PSI, Switzerland

A B S T R A C T

For the R&D of high power spallation targets, one of the key issues is understanding the behavior of structural materials in the severe irradiation environments in spallation targets. At PSI, several experiments have been conducted using the targets of the Swiss spallation neutron source (SINQ) for studying radiation damage effects induced by high energy protons and spallation neutrons. As well, experiments have been performed to investigate liquid lead-bismuth eutectic (LBE) corrosion and embrittlement effects on T91 steel under irradiation with 72 MeV protons. In this paper, an overview will be given showing a selection of results from these experiments, which include the mechanical properties and microstructure of ferritic/maretensitic (FM) steels (T91, F82H, Optifer etc.) and austenitic steels (EC316LN, SS 316L, JPCA etc.) irradiated to doses higher than ever attained by irradiation in a spallation environment, and the behaviors of T91 irradiated with 72 MeV protons in contact with flowing LBE.

1. Introduction

High power (~1 MW or higher) spallation targets are being developed for different attractive applications such as in advanced spallation neutron sources for neutron scattering science and technology or in accelerator driven systems (ADS) for nuclear waste transmutation. In such a target, both, target and structural materials are exposed to intensive irradiation of high energy protons and spallation neutrons. Since the spallation reaction induced by high energy protons can produce helium (He) and hydrogen (H) and other transmutation elements at very high rates, the behavior of materials used in a spallation irradiation environment is expected to be much different from those observed from materials irradiated with neutrons in fission reactors. Therefore, the damage induced by spallation irradiation may not be simply simulated by fission neutron irradiation experiments. To establish a necessary database for the R&D of high power spallation targets, an irradiation experiment was performed at the Los Alamos Neutron Scattering Center (LANSCE) in 1996–1997. Thousands of specimens from SS316L, T91, Inconel 718 etc. were irradiated up to about 12 dpa at ⩽160 °C [1]. To obtain materials data of higher doses and at higher temperatures, the SINQ target irradiation program (STIP) has been run since 1998 within a broad international collaboration with Ecole Polytechnique Federal de Lausanne (EPFL), Forschungszentrum Jülich (FZJ), Oak Ridge National Laboratory (ORNL), Commissariat a L'energie Atomique Centre D'etudes de Saclay (CEA), Japan Atomic Energy Agency (JAEA), Los Alamos National Laboratory (LANL), and University California Santa Barbara (UCSB). The first irradiation experiment (STIP-I) was performed through 1998 and 1999, where more than 1500 samples from nearly 40 kinds of materials were irradiated to doses up to 12 dpa and 1100 appm He (in steels) in a temperature range of about 80 to 400 °C [2]. The second experiment (STIP-II) was conducted in 2000 and 2001, where more than 2000 samples of 40+ kinds of materials were irradiated to doses up to 20 dpa and 1800 appm He in a temperature range of 80 to 450 °C [3]. In 2002 and 2003 the third irradiation experiment (STIP-III) and in 2004 and 2005 the fourth irradiation (STIP-IV) were done. Around 3000 specimens were irradiated to similar doses like that of STIP-II but in a wider temperature range up to 550–600 °C. In the present SINQ target the fifth irradiation (STIP-V) is ongoing. More than 1000 specimens will be irradiated to doses up to 20 dpa and at temperatures up to 700–800 °C.

Due to serious radiation damage effects in solid target materials, using liquid metals as target material becomes more attractive for high power targets. For the pulsed spallation neutron sources in ORNL and JAEA, the target material is liquid mercury (Hg), while for a target used in a continuous spallation source like SINQ or in ADS, liquid lead or liquid lead-bismuth eutectic (LBE) is favored as the target material. Although the use of liquid metals can avoid radiation damage to target materials and does also serve as the primary heat removable medium, liquid metals may introduce additional problems such as corrosion and embrittlement to structural materials [4,5]. It is also well known that radiation may enhance corrosion and embrittlement in environments such as nuclear

* Corresponding author. Tel.: +41 56 310 4171; fax: +41 56 310 4529.
E-mail address: yong.dai@psi.ch (Y. Dai).

0022-3115/$ - see front matter © 2009 Elsevier B.V. All rights reserved.
doi:10.1016/j.jnucmat.2009.02.012

fission reactors. Hence, it is important to investigate liquid metal corrosion and embrittlement effects in spallation irradiation environments. As part of the R&D work supporting the development of a liquid metal target using LBE for SINQ and ADS, namely the so-called Mega-watt-Pilot-Experiment (MEGAPIE) [6,7], the LBE corrosion and embrittlement effects on SS316 and T91 steels under irradiation condition were studied by irradiating some steel specimens in stagnant LBE in STIP and, in particular, in flowing LBE under irradiation with 72 MeV protons. The latter is the so-called LiSoR (liquid–solid-reaction under irradiation) experiments [8].

An overview on the irradiation facilities at PSI was published elsewhere [9], in the present paper, only brief information of the STIP and LiSoR experiments will be given. An overview will be given on the key results obtained from the post-irradiation examinations of STIP I–III and the LiSoR experiments.

2. STIP irradiation and results

2.1. STIP irradiation conditions

Some detailed information of STIP can be found in [2,3]. Hereby a brief introduction is given.

The irradiation is performed in SINQ (solid) targets. Each of them has been operated for two years. Such a target is composed of about 360 rods. A normal target rod is a lead (Pb) rod of about 9.5 mm in diameter clad with either a SS 316L or Zircaloy-2 tube. For STIP irradiations 15–20 target rods in high flux positions are replaced with specimen rods which contain different types of miniature specimens for assessing different mechanical properties such as tensile, fatigue, fracture properties and microstructural analyses, i.e. transmission electron microscopy and small angle neutron scattering etc.

In each target 10 thermocouples are installed to monitor temperatures at different positions. Normally about 5 of them are used for measuring the temperature in specimen rods. The measured values serve as references for calculating the irradiation temperature of the specimens. As the specimens are heated mainly by protons, the temperature (in °C) of a specimen is more or less proportional to the proton flux received. During a two-year operation period, the proton beam current delivered from the accelerator varies as much as 30–40%, which induces correspondingly about a variation in temperature of 30–40%. In addition, the accelerator and multi-target complex inherently experience about 50 to 100 beam trips per day. During beam trips the temperature drops to 40 °C, the temperature of the cooling water. Furthermore, unintended high temperature excursions of up to 20 h duration took place occasionally, which introduced great influence or damage to some specimens of high doses.

The total proton charge received in STIP-I was about 6.7 Ah, while in STIP II–IV it was about 10 Ah. The profile of the accumulated proton fluence, reconstructed by γ-mapping on the beam entrance window of the $AlMg_3$ target container, is approximately a truncated 2D Gaussian distribution with half-widths of about 35 and 25 mm for the major and minor axes, respectively. The proton and neutron fluences received by each specimen, the corresponding dpa values and helium and hydrogen concentrations are calculated with the MCNPX code using this distribution profile. The calculated He concentrations have been corrected based on gas measurements performed at the Pacific Northwest National Laboratory, USA [10,11]. The H concentration cannot be well reproduced because the measured H values show large differences from the calculated values. The difference depends strongly on the irradiation temperature. Those specimens irradiated at >200 °C show much lower measured values, obviously because at these temperatures H diffused out of the specimens.

2.2. Results of STIP irradiation

In last few years a large number of specimens irradiated in STIP-I and STIP-II were analyzed by the STIP partners. The results are published in more than 30 papers in Journal of Nuclear Materials, covering data mostly from FM steels, austenitic steels.

2.2.1. Results from FM steels

As FM steels are selected for key components in MEGAPIE and ADS spallation targets, they are intensively investigated in the related R&D programs. Here the results of tensile and impact tests and TEM observations will be reviewed.

2.2.1.1. Tensile testing results. Tensile tests have been performed on specimens of conventional FM steels T91, EM10, HT9, EP823, and reduced activation steels F82H, Optifer, Optimax [12–17]. Fig. 1 shows the tensile data (YS: yield stress; UTS: ultimate tensile strength; STN: strain-to-necking; TE: total elongation or elongation at fracture) of the steels irradiated in STIP-I and STIP-II to doses between 3 and 20 dpa at temperatures between 80 and 350 °C and tested at room temperature. The data indicate a trend that irradiation hardening increases with dose to about 17 dpa and then starts to saturate. In most of cases, the YS values are very close to the UTS values due to prompt necking of the specimens after irradiation. On the other hand, the ductility decreases significantly, particularly the uniform elongation which drops to about 1% or less in the present dose range. A number of specimens of

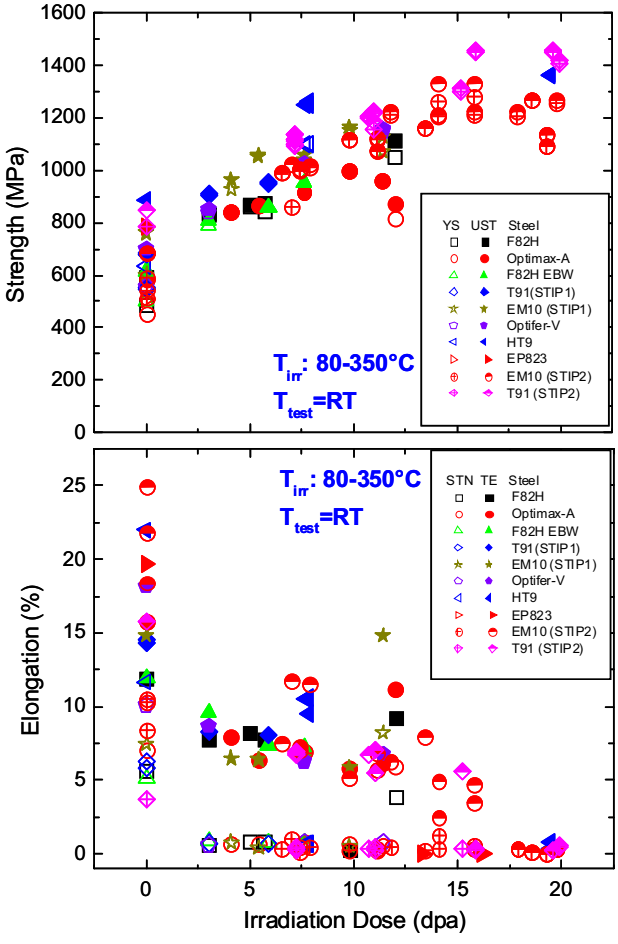

Fig. 1. Tensile data of different FM steels irradiated in STIP-I and STIP-II. The specimens were irradiated at temperatures between 80 and 350 °C and tested at room temperature. The data are compiled from ref. [12–17].

doses above 17 dpa almost completely lost their ductility with a total elongation of less than 2%. The fracture of these specimens shows a mixed mode of inter-granular and cleavage fracture [17]. In the worst case, two EP823 specimens of 13 and 16 dpa and one F82H specimen of about 10 dpa broke in the elastic region [15,16]. Some specimens irradiated in STIP-I to about 12 dpa (the maximum dose of STIP-I) show unexpected large ductility, which is believed to be due to the annealing effects of a high temperature excursion [2,13,16].

Tensile tests have also been performed at higher temperatures up to 400 °C. As an example, Fig. 2 shows the tensile curves of F82H specimens tested at different temperatures close to the average irradiation temperature of the specimens. Due to the effects of higher irradiation and testing temperature, the difference in hardening between specimens of higher and lower doses is reduced. Compared to the specimens tested at room temperature, the specimens tested at higher temperatures show a reduction in strength of 20% or greater. Nevertheless, the hardening and embrittlement effects of the irradiated specimens are still significant. Fig. 3 presents the results of the specimens irradiated in a temperature range of 200–300 °C and tested at 250 °C. It can be seen that, except for a reduction in strength of about 200 MPa, the results show similar features as the results of tests at room temperature shown in Fig. 1.

Up to date, most tensile test results obtained from STIP samples are limited to doses below 15 dpa. In this dose range the STIP data are not much different from those obtained from neutron irradiation, for example those shown in [18,19]. At higher doses, particularly at irradiation temperatures above ~400 °C, the STIP data reveal a substantial hardening not observed in neutron irradiated FM steels, which is a strong indication for helium induced hardening effects [20].

2.2.1.2. Impact testing results. The ductile-to-brittle transition temperature (DBTT) is an important parameter for FM steels, because the DBTT may greatly increase after irradiation. It is well known that the shift of DBTT (ΔDBTT) of different FM steels saturates at a dose level of 1–5 dpa after neutron irradiation [21–23]. Furthermore, some experiments demonstrate that the DBTT shift of FM steels after irradiation may be greatly affected by the helium content produced during irradiation [22,24]. Therefore, He effects on DBTT shift of FM steels are of great concern in fusion and spallation materials programs.

Charpy specimens of either KLST and 1/3 CVN type from different FM steels have been irradiated in STIP to dose up to about 17 dpa at temperature below 300 °C [25,26]. Fig. 4 illustrates the

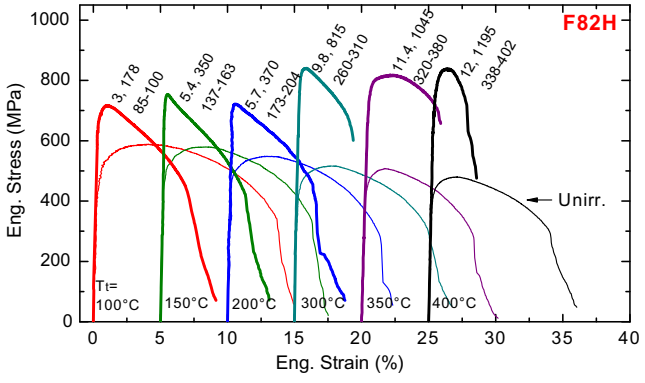

Fig. 2. Engineering tensile stress–strain curves of F82H irradiated in STIP-I and tested at temperatures between 100 and 400 °C. Note: the numbers for each curve indicate the values of dpa, He (appm) and irradiation temperature range. There are shifts of 5% in X-axis for curves obtained at different testing temperatures.

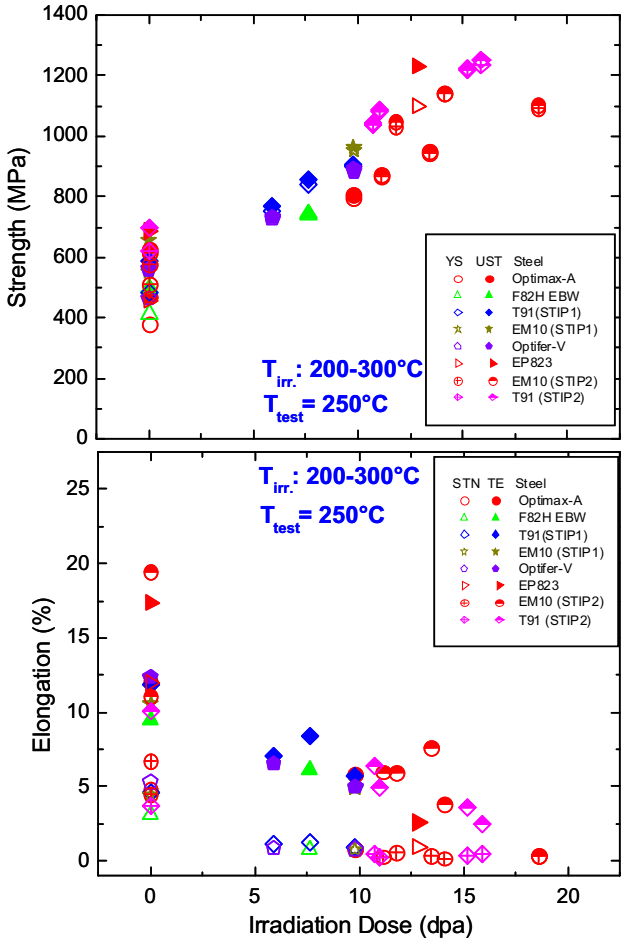

Fig. 3. Tensile data of different FM steels irradiated in STIP-I and STIP-II. The specimens were irradiated at temperatures between 200 and 300 °C and tested at 250 °C. The data are compiled from ref. [12–17].

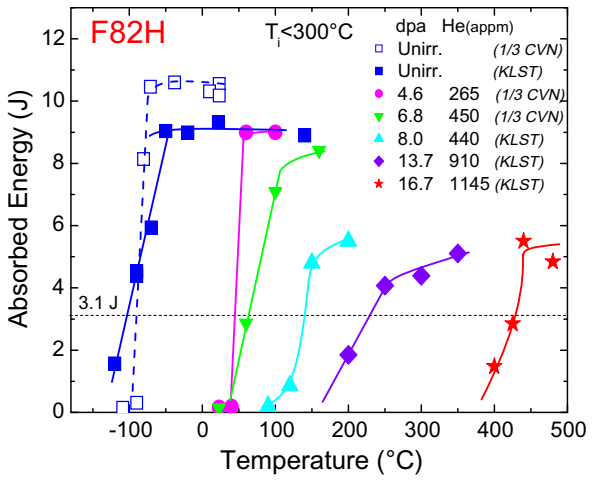

Fig. 4. Charpy impact testing results of F82H specimens (both KLST and 1/3 CVN types) irradiated in STIP to doses between 4.6 and 16.7 dpa.

results of F82H irradiated to doses between 4.6 and 16.7 dpa. It can be seen that the DBTT of the steel increases continuously with dose. An increase of about 515 °C at 16.7 dpa is far beyond that observed in neutron irradiation experiments.

Fig. 5 presents all the ΔDBTT data obtained from the specimens irradiated in STIP-I to STIP-III. Some data obtained from disc small

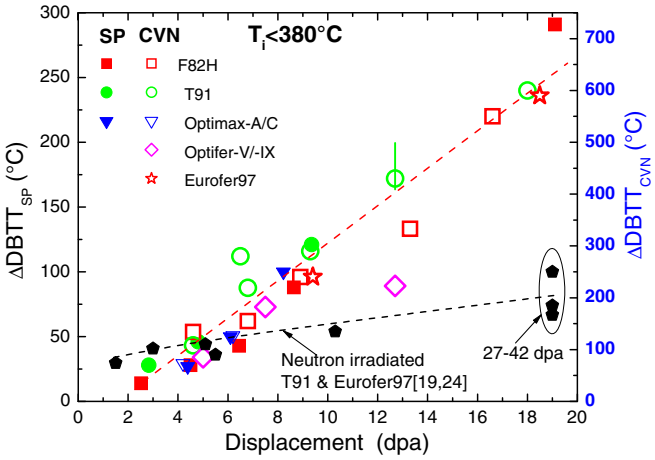

Fig. 5. DBTT shift as a function of irradiation dose for different FM steels irradiated in STIP.

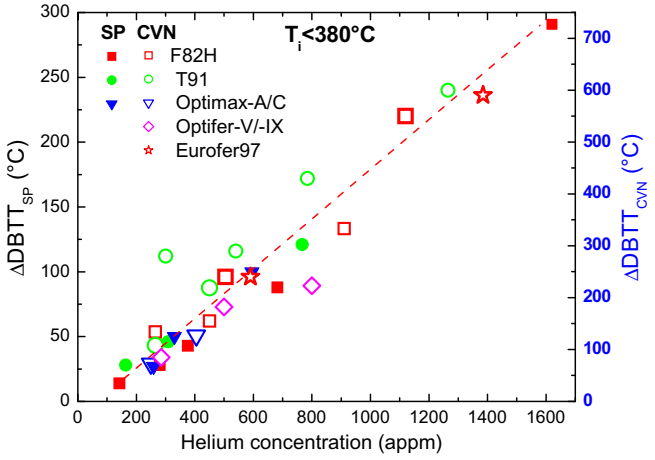

Fig. 6. DBTT shift as a function of helium concentration for both the previous small punch tests [17] and the present Charpy tests.

punch (SP) tests are also included. The SP data ($\Delta DBTT_{SP}$) are converted to Charpy impact data ($\Delta DBTT_{CVN}$) with: $\Delta DBTT_{CVN} = 2.5 \times \Delta DBTT_{SP}$ [27]. For comparison, some data of neutron irradiated T91 and Eurofer 97 [19,24] are included as well. This figure demonstrates clearly that the ΔDBTT of the different FM steels increases more or less linearly with dose after irradiation in spallation environment. At dose of about 5 dpa, the trend of ΔDBTT deviates from that of neutron irradiation, which most likely is attributed to helium effects. The stated helium effects on the DBTT shift can more clearly be seen in Fig. 6 which shows a trend of ΔDBTT proportional to the helium content in the specimens.

The significances of the results are such: (1) helium can cause a very large DBTT shift even much higher than that induced by irradiation hardening effects; (2) the DBTT shift increases more or less linearly with helium concentration; and (3) due to the helium induced DBTT shift, the lifetime of FM steels in fusion reactors and spallation targets where high helium contents are produced can be very limited.

2.2.1.3. TEM investigation results. The irradiation introduced significant changes in the microstructure of the FM steels [28–30]. Irradiation induced defects, namely defect clusters or dislocation loops, were observed in all specimens of doses up to 20 dpa. At $T_i \leqslant 300$ °C, the main features are small defect clusters of 1-2 nm in size and small dislocation loops of a few nm in size. With increasing irradiation dose, the densities of defect clusters and

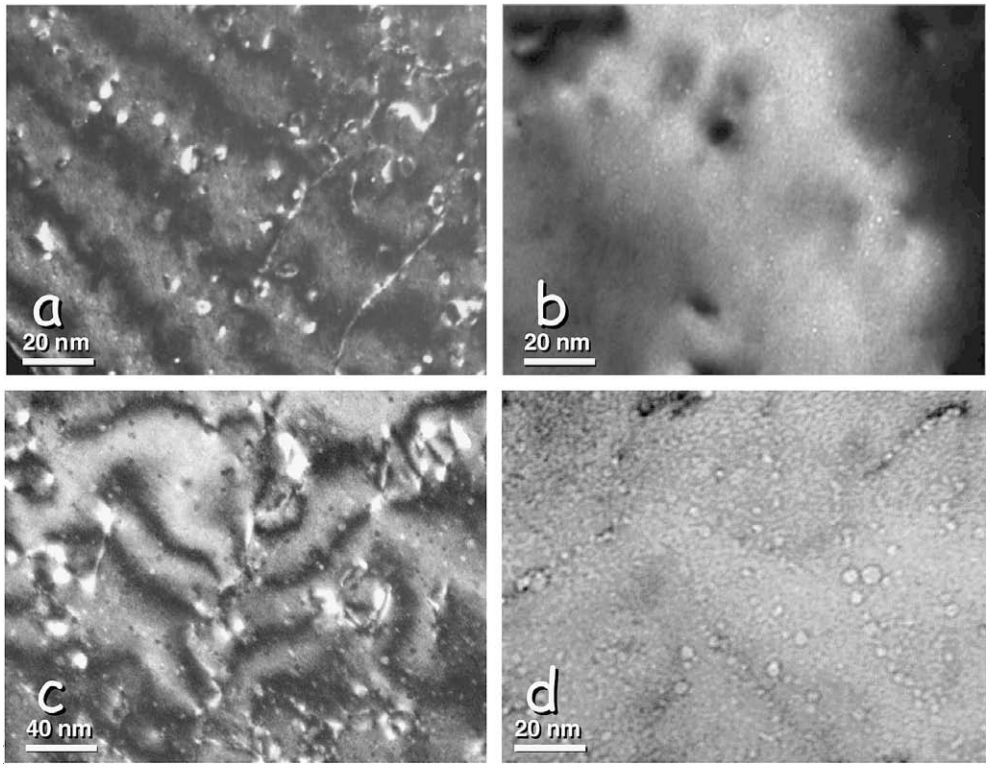

Fig. 7. Dislocation (a and c) and bubble (b and d) structures in F82H specimens irradiated at about 295 and 350 °C to 9.7 and 18.6 dpa, respectively, with 670 and 1400 appm He produced.

loops increase and the size of loops increases as well. At T_i>300 °C, the densities of defect clusters and loops were found decreasing with increasing irradiation temperature. High-density helium bubbles with an average size above 1 nm can be observed in specimens with <~500 appm He and irradiated at ⩽180 °C. With increasing irradiation dose and temperature, the size of bubbles increases.

Fig. 7 illustrates dislocation and bubble structures in two specimens of F82H irradiated to 9.7 and 18.6 dpa with 670 and 1400 appm He and irradiated at about 295 and 350 °C, respectively. In Fig. 7(a) and (b) one can see that in the specimen of 9.7 dpa with 670 appm He, and irradiated at 295 °C, a relatively high density of defect clusters and small loops exists, and very small bubbles are visible, while in the other specimen of 18.6 dpa the densities of both clusters and loops decrease significantly. In fact, most of the small dots (either white or black) in Fig. 7(c) are imaging from bubbles rather than defect clusters. Considering the scale of Fig. 7(c) which is twice that of Fig. 7(a), the loops in the 18.6 dpa specimen are much larger than in the 9.7 dpa specimen. The mean bubble size is about 1.4 and 3.3 nm, respectively, and the bubble density about 4×10^{23} m^{-3} and 3.2×10^{23} m^{-3} in the two specimens. Another difference between the bubble structures of these two specimens is that the bubbles distribute rather homogeneously in the lower dose specimen (Fig. 7(b)), while precipitate preferentially at dislocation lines in the higher dose one (Fig. 7(d)).

Although the microstructure of the irradiated FM steels has been fairly studied, the correlation between microstructure and mechanical properties has not yet well been established. Modeling and more detailed microstructural analyses are needed to deepen the understanding.

2.2.2. Results from austenitic steels

Although SS 316 and SS 304 are widely used in existing spallation targets, the changes of their mechanical properties and microstructure after irradiation in spallation environments still need a better understanding, particularly at high dose levels above 10 dpa and elevated temperatures above 200 °C. Although only limited specimens of different austenitic steels were tested, some interesting results have been obtained.

In the STIP irradiation experiments, four austenitic steels, EC316LN, SS316L, J316F and JPAC have been studied [31–33]. Fig. 8 presents the irradiation dose dependence of the YS, UTS, STN and TE of these steels irradiated to doses up to about 12 dpa in a temperature range of 100–350 °C and tested at room temperature. One can see that the data points of EC316LN, SS316L and JPCA are very close, especially for YS, UTS and TE data. Further-

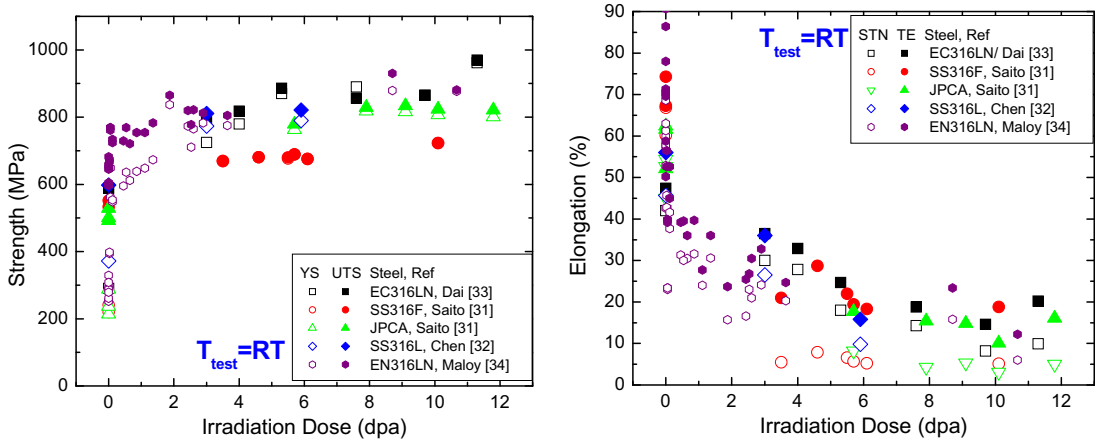

Fig. 8. Irradiation dose dependence of the yield strength (YS), ultimate tensile strength (UTS), strain-to-necking (STN) and total elongation (TE) of austenitic steels irradiated between 100 and 350 °C in STIP-I [31–33] and between 30 and 120 °C in LANSCE [34] tested at room temperature.

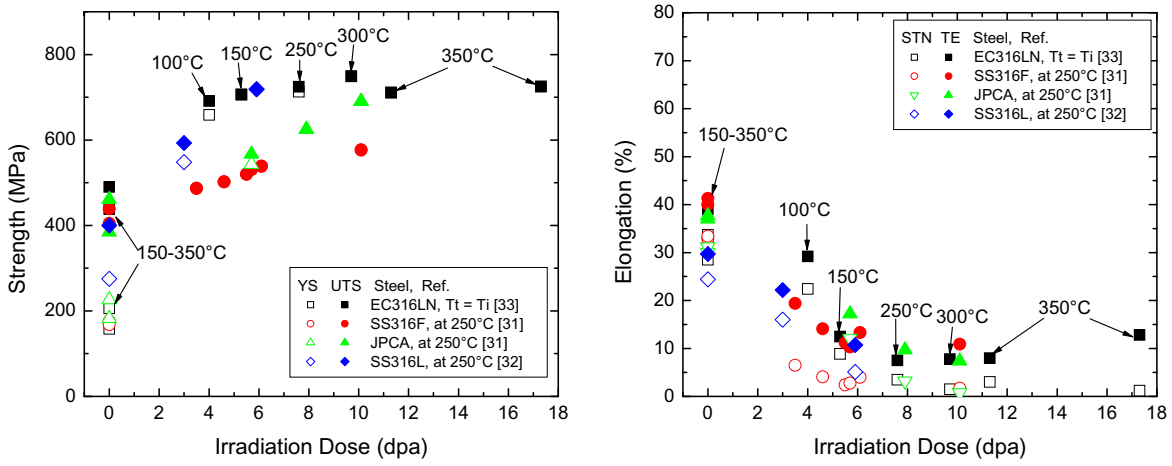

Fig. 9. Irradiation dose dependence of YS, UTS, STN and TE of austenitic steels irradiated in STIP and tested at about the irradiation temperatures between 100 and 350 °C. The testing temperature for SS 316F, JPCA and SS316L is 250 °C.

more, the STIP data are in consistence with the EN316LN data from irradiation performed at LANSCE [34].

Fig. 9 presents the dose dependence of YS, UTS, STN and TE of the four kinds of austenitic steels tested at 100–350 °C. Comparing to Fig. 8, this figure shows that both strength and ductility changes evidently when the testing temperature is increased from 25 to e.g. 150 °C. On the other hand, in the temperature range of 150–350 °C, the changes are much less pronounced, at least for unirradiated specimens. It is believed that between 100 and 350 °C the difference in strength or ductility among the irradiated specimens is mainly induced by irradiation and less affected by the testing temperature.

The tensile results of austenitic steels irradiated in STIP and tested in the temperature range of 150–350 °C are very similar to those of the same steels after neutron irradiation [35]. No substantial difference has been observed in the tensile properties of 316-type steels irradiated in fission reactors and spallation targets in this dose and temperature ranges. This strongly supports the application of austenitic steels in spallation targets. Of course, target design cannot only be based on tensile data. A rather complete database with fracture toughness and fatigue data for these steels is still needed.

The microstructure of the EC316LN steel has been investigated for many irradiation conditions [35], between 2.2 dpa/68 appm He/70 °C and 19.6 dpa/1800 appm He/420 °C. At doses below about 10 dpa and irradiation temperatures below about 300 °C, the results show that the main features of irradiation damage are high-density small "black-dot" defects and large Frank loops. The density and size of the small black-dot defects are little dependent on irradiation dose with a mean size of 1–2 nm and a density of $2–4 \times 10^{23}$ m^{-3}. For Frank loops, the density varies little with dose, while the size increases with dose. No bubbles or voids were observed except in a specimen irradiated at above ~350 °C, where high-density small bubbles were found.

Fig. 10 shows a bright-field (BF) and a weak-beam-dark-field (WBDF) images of an area in the specimen irradiated to 12.8 dpa/1010 appm He at 273±30 °C. The mean size of the defect clusters is about 1.6 nm and their density is about 3.2×10^{23} m^{-3}. The mean size of the loops is about 13.5 nm and the density of the loops is about 2.5×10^{22} m^{-3}. In this specimen, no bubbles or cavities could be resolved.

Fig. 11 illustrates the microstructure of the specimen irradiated to 19.6 dpa/1800 appm He at 420 ± 55 °C. The features of defect clusters and loops are similar to that shown in Fig. 10. The main

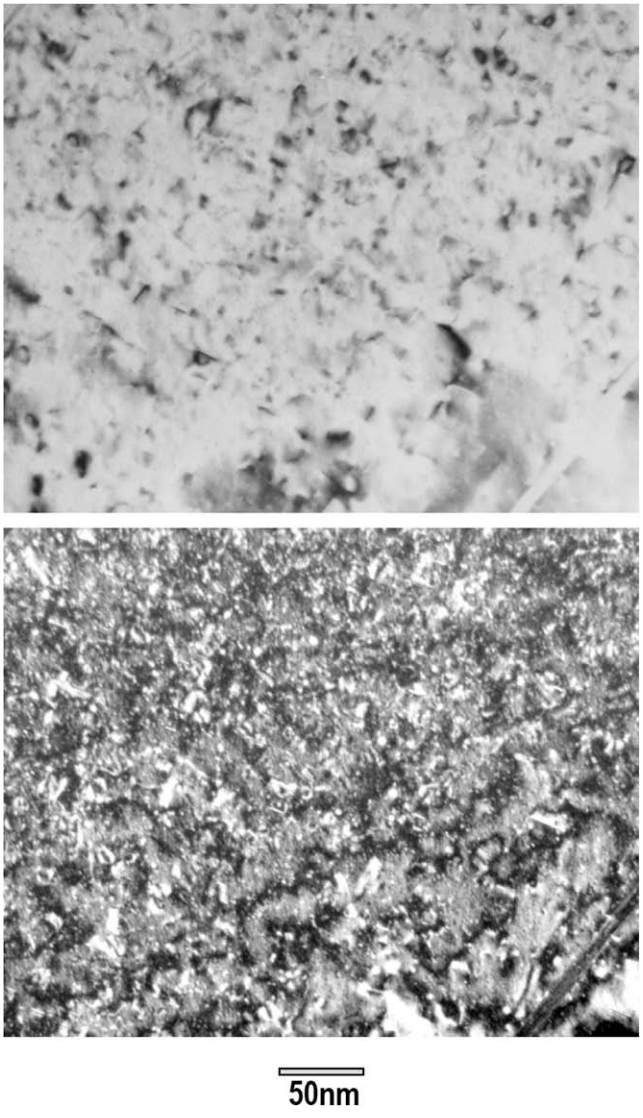

Fig. 10. BF (upper) and WBDF (lower) images showing the defect structure in the SS 316LN specimen irradiated to 12.8 dpa / 1010 appm He at 273±30 °C.

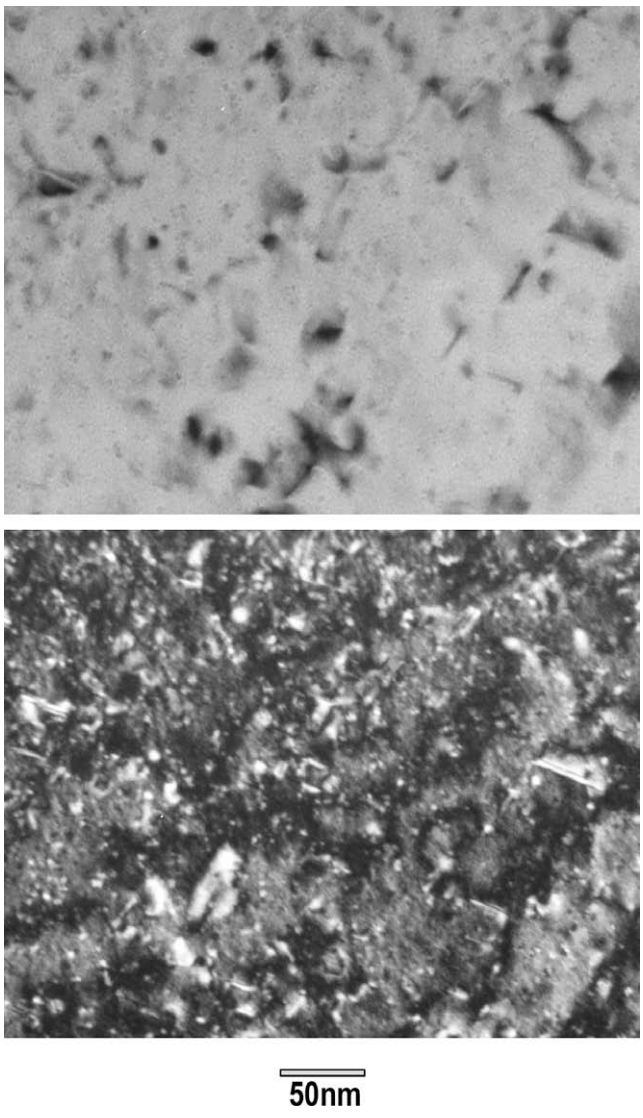

Fig. 11. BF (upper) and WBDF (lower) images showing the defect structure in the SS 316LN specimen irradiated to 19.6 dpa / 1800 appm He at 420±55 °C.

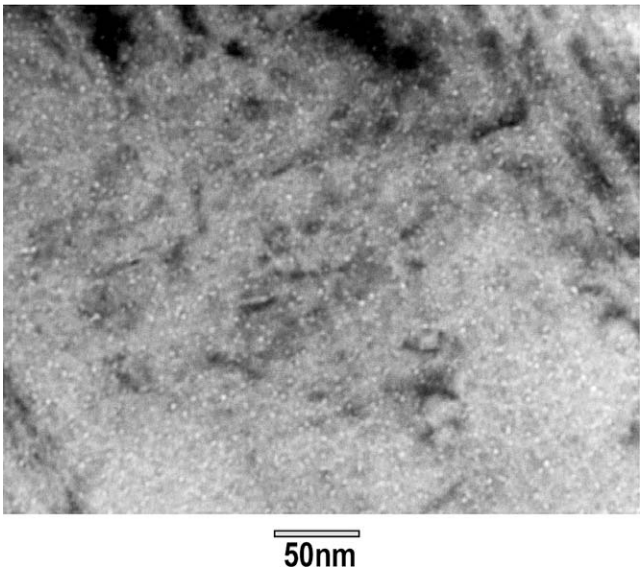

Fig. 12. De-focused BF image showing helium bubbles formed in the SS 316LN specimen irradiated to 19.6 dpa / 1800 appm He at 420±55 °C.

difference is that small bubbles of high density were observed, as demonstrated in Fig. 12. Small bubbles of about 2 nm formed in the specimen at a high density of about 5×10^{23} m^{-3}, distributed homogeneously in the matrix. No preferential precipitation of bubbles was observed.

In general, the hardening observed in tensile tests is attributed to the defect clusters, dislocation loops and helium bubbles (even not visible ones). However, it is suspected the most of the helium bubbles may be associated with defect clusters and dislocation loops (e.g. Fig. 7(d)) due to strong attractive interaction between helium and point defects and dislocations. In this case, the classical knowledge of hardening effects from "pure" defect clusters, dislocation loops, and He-bubbles may not be sufficiently comprehensive. A more specific understanding of hardening effects of complexes such as defect clusters with He bubbles and dislocation loops with He bubbles is needed.

3. LiSoR irradiation and results

LiSoR is a unique facility to investigate simultaneously the influence of flowing LBE, static mechanical stress and additional fluctuating thermal stress under irradiation of a steel probe. The LiSoR facility is actually a LBE loop installed at a proton beam line of Injector-I at PSI. The energy of the proton beam is 72 MeV. The material selected for Lisor experiments was T91 steel which was the LBE container material for the MEGAPIE target. The detailed information of the experimental setup can be found in [8].

3.1. LiSoR irradiation conditions

Up to date six experiments were conducted. The irradiation conditions in two important parts, the proton beam entrance window of the tube and the irradiation area of the inner specimen, of each test section (TS), except for that of Lisor-1, are list in Table 1. The outstanding values of temperature and stress of LiSoR-2 were induced by a too small beam spot and by wobbling the proton beam at a too low frequency of about 2 Hz [36].

It should be pointed out that there was no control of the oxygen content in the LBE due to its low temperature. The oxygen content can be considered as the oxygen saturation level at 300 °C which is about the temperature in the storage tank. Another point to be mentioned is that for studying corrosion effects on coated T91 steel, both outer and inner surfaces of the TS-tube of Lisor-6 were coated with TiN using the plasma coating technique [37], while its TS-specimen was one-side treated with Al-alloying using the GESA technique [38].

Table 1
Irradiation conditions of LiSoR-2 to Lisor-6.

	LiSoR-2	LiSoR-3	LiSoR-4	LiSoR-5	LiSoR-6
Irradiation time (h)	34	264	144	724	~1900
Averaged proton energy					
TS-tube (MeV)	70	70	70	70	70
TS-specimen (MeV)	40	40	40	40	40
Beam current (μA)	50	15	30	30	30
Peak oscillating temperature at LBE contacting surface					
TS-tube (°C)	650	330	400	400	400
TS-specimen (°C)	580	324	380	380	380
Peak oscillating temperature in bulk					
TS-tube (°C)	>700	380	550	550	550
TS-specimen (°C)	>600	345	440	440	440
Maximum stress					
TS-tube (°C)	>150	25	75	75	75
TS-specimen (°C)	200	200	200	200	200
Irradiation dose					
TS-tube (dpa)	0.1	0.2	0.2	1.0	2.5
TS-specimen (dpa)	0.075	0.15	0.15	0.75	1.8
He concentration					
TS-tube (appm)	3.6	7.2	7.2	36	90
TS-specimen (appm)	2.6	5.2	5.2	26	65

3.2. Surface inspection results

The photos of the visual inspection were taken from the irradiation areas of both the TS-tubes and the TS-specimens of the five irradiations, as shown in Fig. 13. In the upper photos, except for that of Lisor-6, the beam foot print on each TS-tube can clearly be seen. In the LiSoR-2 TS-tube, a crack was formed due to high temperature and high thermal stress induced by a too small beam size [39]. The LBE on LiSoR-2 TS-tube was leaking out from the crack. No evident damages were observed in other TS-tubes. On the surfaces of the TS-specimens (Fig. 13, lower photos) one can see some remaining of LBE. On the TS-specimens of LiSoR-2 and -5 a significant amount of adherent LBE is visible. Only little traces of LBE could be seen on the other TS-specimens, particularly in Lisor-6 the coating seems not wetted by LBE even after irradiation. The irradiation areas in LiSoR-2 and -5 specimens are quite easy to recognize, while those of LiSoR-3, -4 and -6 are more difficult.

After the visual inspection, the TS-tubes and TS-specimens were cut with an EDM machine into small dog-bone shaped tensile samples for tensile testing, and the remaining pieces between the tensile samples were saved for TEM, SEM, SIMS, etc. analyses.

SEM (for low activity samples) or EPMA (for high activity samples) analyses were performed to inspect the surface after irradiation in contact with LBE. Except for slight oxidation (1–5 μm thick oxide layers) observed on the surfaces in the irradiation areas, no evident corrosion effects were detected [39,40]. As for the TiN and GESA coating, slight damage was observed in the TiN coating layer and almost no change was seen in the GESA coating [41].

3.3. Tensile testing results

As mentioned above, one of the main purposes of the LiSoR experiments was to investigate the LBE embrittlement effects on T91 steel under irradiation. None of the TS-specimens was broken during irradiation, although a mechanical loading of 200 MPa were always applied. This is at least a good indication that shows that

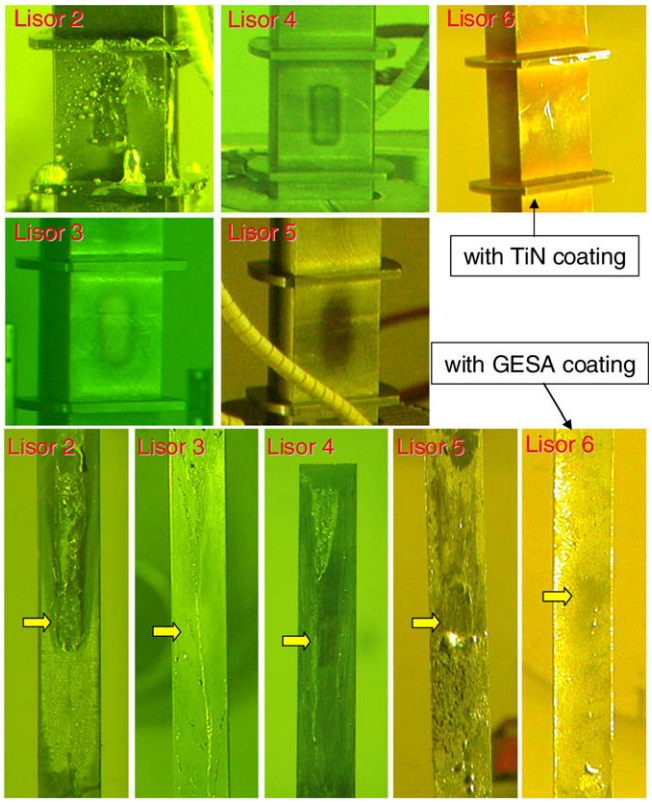

Fig. 13. Photos show the TS-tubes (upper) and TS-specimens (lower) of LiSoR-2 to -6 after irradiation. The arrows indicate the irradiation areas.

the material can withstand such mechanical load to a radiation damage level of about 1.8 dpa. To analyze the actual degradation of mechanical properties induced by LBE and irradiation, tensile tests were performed. The samples were divided into two groups. The first group samples were tested in Ar atmosphere. The results of these tests should represent the status of the T91 steel after irradiation in LiSoR. The second group samples were tested in LBE. These tests were intended to show additional effects from the testing environment in LBE. All the tests were performed at 300 °C [42].

Fig. 14 presents the tensile results of some LiSoR-3 and LiSoR-5 samples tested in Ar. The samples from the irradiation area of the TS-specimens demonstrate slight hardening induced by irradiation as expected (a and c). However, the hardening in the samples from the irradiation area of the TS-tubes is much less (b and d). This is due to the fact that the temperature in the irradiation area of the TS-tubes was higher $\geqslant$350 °C, where irradiation hardening effects in martensitic steels are less significant. The ductility is only slightly reduced in samples of LiSoR-3, and more strongly in LiSoR-5. Our studies of LBE embrittlement effects on FM steels suggest that the strong reduction in ductility of LiSoR-5 samples is mostly due to the embrittlement by LBE during tensile testing rather than during irradiation. As can be seen in Fig. 13, some LBE adhered on the surface of the TS-specimen of LiSoR-5. During EDM cutting or testing, the LBE could enter the microcracks on the side surfaces of the samples, which were produced by EDM cutting, and finally induced the embrittlement effects. As LBE embrittlement effects become more pronounced with increasing strength of FM steels [43], it is understandable that the Lisor-5 samples of higher doses show greater reduction than the Lisor-3 samples.

The significances of the Lisor experiments are that: (1) LBE corrosion under the MEGAPIE relevant irradiation condition is not so serious, at least up to 2-3 dpa; (2) FM steels like T91 can withstand relatively high stress of 200 MPa in flowing LBE under severe irradiation; and (3) with proper coating, the resistance of FM steels to LBE corrosion can be increased.

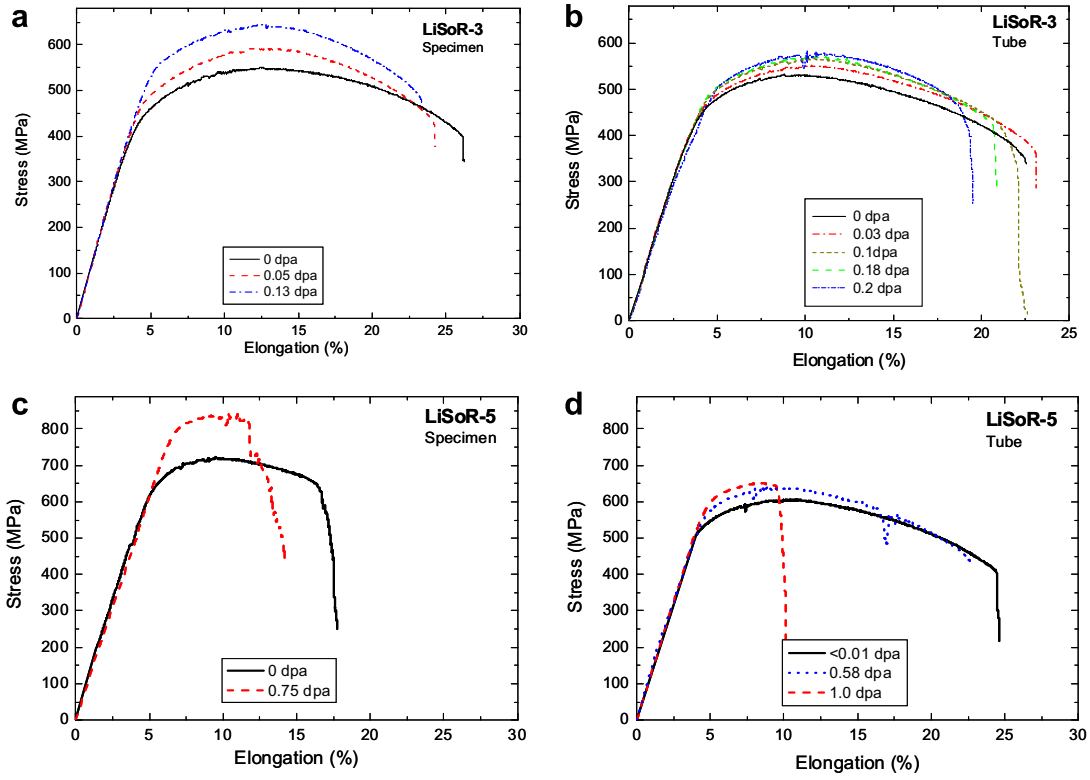

Fig. 14. Tensile results of some LiSoR-3 and LiSoR-5 samples tested at 300 °C in Ar.

4. Summary and outlook

In this paper, only part of the STIP and Lisor results could be described above, mostly from tensile testing and TEM investigations on FM steels and austenitic steels. A rather complete collection of STIP and Lisor results can be found in the proceedings of the last five International Workshop on Spallation Materials and Technology (IWSMT), published in Journal of Nuclear Materials volumes 296, 318, 343, 356, and another one in press now. Much more data such as fracture toughness and fatigue properties will be generated, and other metals and alloys such as Al-, Ni-, and Zr-alloys will be studied in detail. Furthermore, the post irradiation examinations of the MEGAPIE target is planned, which will provide unique information from T91 and SS 316L steels under intensive irradiation with a spallation spectrum in flowing LBE.

References

[1] S.A. Maloy et al., J. Nucl. Mater. 296 (2001) 119.
[2] Y. Dai, G.S. Bauer, J. Nucl. Mater. 296 (2001) 43.
[3] Y. Dai et al., J. Nucl. Mater. 343 (2005) 33.
[4] F. Barbier, A. Rusanov, J. Nucl. Mater. 296 (2001) 231.
[5] G. Nicaise, A. Legris, J.B. Volg, J. Foct, J. Nucl. Mater. 296 (2001) 256.
[6] G.S. Bauer, M. Salvatores, G. Heusener, J. Nucl. Mater. 296 (2001) 17.
[7] Werner Wagner, Friedrich Gröschel, Knud Thomsen, Hajo Heyck, J.Nucl. Mater. in press.
[8] T. Kirchner et al., J. Nucl. Mater. 318 (2003) 70.
[9] Werner Wagner, Yong Dai, Heike Glasbrenner, Hans-Ulrich Aebersold, J. Nucl. Mater. 361 (2007) 274.
[10] Y. Dai, Y. Foucher, M.R. James, B.M. Oliver, J. Nucl. Mater. 318 (2003) 167.
[11] B.M. Oliver, Y. Dai, R.A. Causey, J. Nucl. Mater. 356 (2006) 148.
[12] Y. Dai, X. Jia, K. Farrell, J. Nucl. Mater. 318 (2003) 192.
[13] J. Henry, X. Averty, Y. Dai, P. Lamagnere, J.P. Pizzanelli, J.J. Espinas, P. Wident, J. Nucl. Mater. 318 (2003) 215.
[14] J. Chen, M. Rödig, F. Carsughi, Y. Dai, G.S. Bauer, H. Ullmaier, J. Nucl. Mater. 343 (2005) 236.
[15] Stuart A. Maloy, T. Romero, M.R. James, Y. Dai, J. Nucl. Mater. 356 (2006) 56.
[16] Y. Dai, G.W. Egeland, B. Long, J. Nucl. Mater., in press.
[17] J. Henry, X. Averty, Y. Dai, J.P. Pizzanelli, J. Nucl. Mater., in press.
[18] A.F. Rowcliffe et al., J. Nucl. Mater. 258–263 (1998) 1275.
[19] A. Alamo, J.L. Bertin, V.K. Shamardin, P. Wident, J. Nucl. Mater. 367–370 (2007) 53.
[20] Z. Tong, Y. Dai, to be published.
[21] D.S. Gelles, J. Nucl. Mater. 149 (1987) 192.
[22] M. Rieth, B. Dafferner, H.D. Röhrig, J. Nucl. Mater. 258–263 (1998) 1147.
[23] R.L. Klueh, D.J. Alexander, J. Nucl. Mater. 258–263 (1998) 1269.
[24] R.L. Klueh, D.J. Alexander, J. Nucl. Mater. 187 (1992) 60.
[25] Yong Dai, Pierre Marmy, J. Nucl. Mater. 343 (2005) 247.
[26] Y. Dai, to be published.
[27] X. Mao, H. Takahashi, J. Mater. Sci. 27 (1992) 983.
[28] X. Jia, Y. Dai, M. Victoria, J. Nucl. Mater. 305 (2002) 1.
[29] X. Jia, Y. Dai, J. Nucl. Mater. 343 (2005) 212.
[30] X. Jia, Y. Dai, J. Nucl. Mater. 356 (2006) 105.
[31] S. Saito, K. Kikuchi, K. Usami, A. Ishikawa, Y. Nishino, M. Kawai, Y. Dai, J. Nucl. Mater. 343 (2005) 253.
[32] J. Chen, M. Roedig, F. Carsughi, Y. Dai, G.S. Bauer, H. Ullmaier, J. Nucl. Mater. 343 (2005) 236.
[33] Y. Dai, G.W. Egeland, B. Long, J. Nucl. Mater. 377 (2008) 109.
[34] S.A. Maloy, M.R. James, W.R. Johnson, T.S. Byun, K. Farrell, M.B. Toloczko, J. Nucl. Mater. 318 (2003) 283.
[35] D. Hamaguchi, Y. Dai, J. Nucl. Mater. 343 (2005) 262.
[36] K. Samec, PSI Technical Report, TM-34-05-02.
[37] H. Glasbrenner, F. Groeschel, J. Nucl. Mater. 356 (2006) 213.
[38] V. Engelko, B. Yatsenko, G. Mueller, H. Bluhm, Vacuum 62 (2001) 211.
[39] Y. Dai, H. Glasbrenner, V. Boutellier, R. Bruetsch, X. Jia, F. Groeschel, J. Nucl. Mater. 335 (2004) 232.
[40] H. Glasbrenner, R. Bruetsch, Y. Dai, F. Groeschel, M. Martin, J. Nucl. Mater. 356 (2006) 247.
[41] D. Gavillet, M. Martin, Y. Dai, J. Nucl. Mater. 377 (2008) 213.
[42] Y. Dai, B. Long, X. Jia, H. Glasbrenner, K. Samec, F. Groeschel, J. Nucl. Mater. 356 (2006) 256.
[43] B. Long, Z. Tong, F. Groeschel, Y. Dai, J. Nucl. Mater. 377 (2008) 219.